JGR Space Physics

RESEARCH ARTICLE
10.1029/2025JA034892

Statistical Investigation of the Interplay Between Chorus and Electron Cyclotron Harmonic Waves

Jiuqi Ma[1,2], Xinliang Gao[1,2], Quanming Lu[1,2], Tong Shao[1,2], Yangguang Ke[3], and Xuan Zhou[1,2]

[1]School of Earth and Space Sciences, University of Science and Technology of China, Hefei, China, [2]Deep Space Exploration Laboratory, University of Science and Technology of China, Hefei, China, [3]School of Energy Science and Engineering, Harbin Institute of Technology, Harbin, China

Key Points:

- Chorus and ECH waves frequently coexist, with co-occurring events having higher rates and larger amplitudes than either alone
- Co-occurring events show a clear anticorrelation in amplitudes, indicating that their interplay is common in Earth's magnetosphere
- The amplitude ratio E_{chorus}/E_{ech} decreases with increasing f_{pe}/f_{ce} and hot electron density, consistent with simulation results

Supporting Information:

Supporting Information may be found in the online version of this article.

Correspondence to:

X. Gao,
gaoxl@ustc.edu.cn

Citation:

Ma, J., Gao, X., Lu, Q., Shao, T., Ke, Y., & Zhou, X. (2026). Statistical investigation of the interplay between chorus and electron cyclotron harmonic waves. *Journal of Geophysical Research: Space Physics*, *131*, e2025JA034892. https://doi.org/10.1029/2025JA034892

Received 23 NOV 2025
Accepted 24 FEB 2026

Abstract Whistler-mode chorus and electrostatic electron cyclotron harmonic (ECH) waves are fundamental plasma modes in Earth's magnetosphere that play crucial roles in radiation belt dynamics. While their individual characteristics have been extensively investigated, systematic statistical analyses of their interplay and its dependence on ambient plasma conditions remain scarce. Using observations from the Van Allen Probes between October 2012 and December 2014, we identified 8,750 ECH-only, 4,215 chorus-only, and 12,467 co-occurring events. Simultaneous chorus and ECH waves are frequently observed near the magnetic equator, primarily in the midnight-to-dawn sector at L-shells between 4 and 6. These co-occurring events are more prevalent and display stronger wave amplitudes than intervals in which only one wave type is present. During co-occurring intervals, their amplitudes exhibit a clear anticorrelation, indicating that chorus-ECH interactions are ubiquitous in the Earth's magnetosphere. Moreover, the amplitude ratio between chorus and ECH waves decreases with increasing plasma-to-cyclotron frequency ratio (f_{pe}/f_{ce}) and hot electron density but shows little dependence on electron temperature anisotropy or parallel plasma beta. These findings provide new statistical evidence for the widespread occurrence of chorus-ECH interactions and highlight their significance for electron dynamics and space weather modeling.

Plain Language Summary The Earth's magnetosphere contains various types of plasma waves that control the behavior of energetic electrons in the radiation belts. Two of the most important wave types are whistler-mode chorus and ECH waves. Recent studies show that chorus waves suppress ECH waves by using up the free energy associated with the temperature anisotropy and loss cone instabilities; however, whether such interplay is a common phenomenon in the Earth's magnetosphere remains unclear. Using data from the Van Allen Probes, we find that these two wave types often appear together, particularly near the magnetic equator from midnight to dawn. When they occur simultaneously, their amplitudes exhibit a clear anticorrelation. We further find that the surrounding plasma environment plays a significant role in regulating this relationship: the amplitude ratio between chorus and ECH waves decreases as the ratio of plasma frequency to electron cyclotron frequency increases and as the hot electron density increases. These results not only provide evidence that the interplay between chorus and ECH waves is a common phenomenon but also contribute to advancing models of radiation belt dynamics and space weather forecasting.

1. Introduction

Whistler-mode chorus waves and electrostatic electron cyclotron harmonic (ECH) waves are two of the most prominent plasma wave modes in Earth's magnetosphere, both playing vital roles in regulating the dynamics of energetic electrons (Anderson & Maeda, 1977; Helliwell, 1967; Horne et al., 1981, 2005; Kennel et al., 1970; Ni et al., 2016; Nishimura et al., 2010). Chorus waves are right-hand circularly polarized electromagnetic emissions typically observed between 0.1 and 0.8 f_{ce}, where f_{ce} is the electron cyclotron frequency (Burtis & Helliwell, 1976; Tsurutani & Smith, 1977). They can accelerate ~100 keV electrons to relativistic energies, serving as a major source of relativistic electrons in the radiation belts (Thorne et al., 2013; Tu et al., 2014; Xiao et al., 2014). In addition, chorus waves effectively scatter electrons into the upper atmosphere, producing microbursts and diffuse auroras (R. Chen et al., 2024; Feng et al., 2024; Thorne et al., 2010; Tsurutani et al., 2013). The net effect of these processes is energy-dependent and is also critically sensitive to the latitudinal distribution of the waves (Wang & Shprits, 2019). A characteristic power minimum near 0.5 f_{ce} divides chorus into a lower band (0.1–0.5 f_{ce}) and an upper band (0.5–0.8 f_{ce}) (H. Chen et al., 2022, 2021; J Li et al., 2022; Tsurutani & Smith, 1974). Chorus emissions

typically appear as quasi-periodic, discrete elements with frequency chirping (Gao et al., 2022, 2014; W. Li et al., 2012; Tsurutani et al., 2020). Both theoretical and observational studies indicate that chorus is generated near the geomagnetic equator, with free energy supplied by the temperature anisotropy of energetic electrons injected from the magnetotail plasma sheet (DeForest & McIlwain, 1971; LeDocq et al., 1998; Omura et al., 2008; Tao et al., 2019; Tsurutani et al., 1979). The repetitive generation of chorus reflects continuous injections of energetic electrons (Gao et al., 2022; Lu et al., 2021), and its frequency chirping arises from nonlinear wave–particle interactions (Ke et al., 2020; Omura, 2021). The occurrence and intensity of chorus are strongly modulated by geomagnetic substorms, and chorus is primarily observed outside the plasmasphere over a broad magnetic local time (MLT) range of 22:00–13:00, consistent with the eastward drift of injected electrons (W. Li et al., 2009; Ma et al., 2022; Meredith et al., 2003; Tsurutani & Smith, 1977; Wang et al., 2019).

ECH waves are electrostatic emissions with frequencies located between successive harmonics of f_{ce} (Fredricks & Scarf, 1973; Kennel et al., 1970). They resonate most efficiently with ∼0.1–10 keV electrons, rapidly scattering them into the loss cone and thereby contributing to diffuse auroral precipitation (Fukizawa et al., 2020; Horne et al., 2003; Lou et al., 2021; Ni et al., 2012; Zhang et al., 2015). ECH waves are generally driven by the loss-cone instability of hot electrons (Ashour-Abdalla & Kennel, 1978; Liu et al., 2018; Wu et al., 2020), with occurrence rates peaking in the midnight-to-dawn sector (21:00–06:00 MLT) at L-shells between 4 and 10 (Lou et al., 2025; Ni et al., 2017). Because ECH waves propagate nearly perpendicular to the ambient magnetic field, they are typically confined near the magnetic equator. However, recent studies indicate that this confinement depends on the L-shell. For instance, Lou et al. (2025) showed that at high L-shells ($L > 8$), ECH waves can be observed over a broad latitudinal range of $|\mathrm{MLAT}| < 35°$, particularly on the pre-noon side. Similar to choruses, their occurrence rate and intensity increase with enhanced geomagnetic activity (Meredith et al., 2009; Ni et al., 2016).

The similar occurrence patterns and comparable amplitudes of chorus and ECH waves naturally raise the question of whether these two wave modes evolve independently. Recent studies have revealed an inverse correlation between their intensities, implying that chorus can suppress ECH waves and thereby account for the dominant role of chorus in driving diffuse auroral precipitation (Gao et al., 2024). Combined observations and simulation results suggest that this suppression arises from loss-cone filling due to chorus-induced electron scattering, implying that the instability responsible for generating chorus waves consumes the available free energy and thereby suppresses the growth of ECH waves. Numerical simulations further demonstrate that this suppression can occur under a broad range of plasma conditions, and that the amplitude ratio of ECH to whistler-mode waves increases with an increasing fraction of hot electrons and a higher ratio of plasma frequency to electron cyclotron frequency (Shao et al., 2025). Nevertheless, direct observational evidence confirming the ubiquity of chorus-ECH interactions and their dependence on ambient plasma parameters remains limited.

In this study, we present a comprehensive statistical analysis of the relationship between chorus and ECH waves using data from the Van Allen Probes collected between October 2012 and December 2014. Our results demonstrate that the two wave modes frequently occur simultaneously and exhibit a clear anticorrelation in amplitude. The remainder of this paper is organized as follows: Section 2 describes the data sets and analysis methods, Section 3 presents the statistical results, and Sections 4 and 5 discuss and summarize the main findings.

2. Data and Analysis Methods

2.1. Data Sets

We utilize electric field, magnetic field, and plasma measurements from the twin Van Allen Probes spacecraft (Kessel et al., 2013; Mauk et al., 2012), which operated from August 2012 to October 2019 in near-equatorial, elliptical orbits (perigee ∼1.1 R_E, apogee ∼5.8 R_E). Wave observations were obtained from the Electric and Magnetic Field Instrument Suite and Integrated Science (EMFISIS) suite (Kletzing et al., 2013). Survey-mode spectral matrices with a 6 s resolution over the frequency range 10 Hz–12 kHz were analyzed to derive wave power spectral densities and polarization parameters. The background magnetic field (B_0) is measured by the tri-axial fluxgate magnetometer (MAG) and used to calculate the local electron cyclotron frequency (Kletzing et al., 2013). The electron plasma density is determined from the upper hybrid resonance frequency measured by the high-frequency receiver (HFR (Kurth et al., 2015);). Electron fluxes are obtained from the Helium, Oxygen, Proton, and Electron (HOPE) instrument and the Magnetic Electron Ion Spectrometer (MagEIS), both part of the Energetic Particle, Composition, and Thermal Plasma (ECT) suite (Spence et al., 2013). Together, these instruments cover an energy range from a few eV to several MeV (Blake et al., 2013; Funsten et al., 2013).

Spacecraft positions are mapped into geomagnetic coordinates (L, MLT, magnetic latitude (MLAT)) using the TS04 magnetic field model (Tsyganenko & Sitnov, 2005).

2.2. Wave Identification

Wave events are identified using data from both Probe A and Probe B between October 2012 and December 2014. Chorus waves are selected when their frequencies fall within 0.1–0.8 f_{ce}, with both wave planarity and ellipticity greater than 0.7, and with magnetic and electric field amplitudes exceeding 0.002 nT and 0.03 mV/m, respectively (Ma et al., 2022). The chorus magnetic and electric amplitudes are calculated as the root mean square (RMS) of the integrated magnetic and electric spectral densities over 0.1 to 0.8 f_{ce}. ECH waves are identified when the electric power spectral density exhibits enhancements within 1–2 f_{ce} and the electric wave amplitude exceeds 0.03 mV/m (Ni et al., 2017), where the ECH wave amplitude is computed as the RMS of the integrated electric spectral density over 1–2 f_{ce}. To ensure that both wave types are observed outside the plasmasphere, we restrict the analysis to intervals with plasma densities below 30 cm^{-3} and $L > 3$ (Sheeley et al., 2001).

2.3. Plasma Parameters

To characterize the background plasma environment, we derive the temperature and hot electron density of the source population from the electron velocity distribution functions. The hot electron velocity distribution is modeled using a bi-Maxwellian function (Kubota et al., 2018):

$$F(v,\alpha) = F_0 \exp\left(-\frac{mv^2 \cos^2\alpha}{2T_\parallel} - \frac{mv^2 \sin^2\alpha}{2T_\perp}\right), \tag{1}$$

where

$$F_0 = n_0 \sqrt{\frac{m}{2\pi T_\parallel}}\ \frac{m}{2\pi T_\perp},$$

and $T_\parallel$ and $T_\perp$ are the parallel and perpendicular temperatures, respectively, while m, n_0, v and α represent the electron mass, density, total speed, and pitch angle, respectively. The fitting procedure is performed within the resonant velocity range (ΔV_r) relevant to chorus wave interactions. The resonant velocity range is determined from the nonrelativistic first-order resonance condition: $V_r = \frac{2\pi(f_w - f_c)}{k}$, where f_w corresponds to the lower and upper frequency bounds of the chorus wave band, k is the wave number derived from the cold plasma dispersion relation (Stix & Scott, 1963), and f_c is the electron cyclotron frequency.

The fitting was carried out in two steps. First, substituting $\alpha = 90°$ into the distribution function yields:

$$F(v,90°) = F_0 \exp\left(-\frac{mv^2}{2T_\perp}\right), \tag{2}$$

which can be expressed in logarithmic form as

$$\ln F(v,90°) = \ln F_0 - \frac{mv^2}{2T_\perp}. \tag{3}$$

By fitting the observed phase space densities at $\alpha = 90°$ to the above equation over the resonant velocity range, we obtain the perpendicular temperature $T_\perp$. In the second step, we fit the phase space density over the corresponding resonant velocity range to the general form:

$$\ln F(v,\alpha) = \ln F_0 - \frac{mv^2 \cos^2\alpha}{2T_\parallel} - \frac{mv^2 \sin^2\alpha}{2T_\perp}. \tag{4}$$

The parallel temperature is derived from the slope corresponding to $\frac{m}{2T_{\parallel}}$, and the hot electron density n_h is obtained from the intercept ln F_0. The temperature anisotropy is defined as $A = T_{\perp}/T_{\parallel}$. To ensure reliability, only results satisfying $0.75 < (\ln F_0)_{\text{step1}}/(\ln F_0)_{\text{step2}} < 1.25$ are retained for analysis.

3. Statistical Results

Figure 1 shows a representative interval observed by Probe A on 8 October 2014, illustrating (a) electron number density, (b) magnetic field power spectral density, (c) electric field power spectral density, (d) electric amplitude of chorus waves, (e) electric amplitude of ECH waves, (f) the ratio of plasma frequency to electron cyclotron frequency (f_{pe}/f_{ce}), (g) hot electron density, (h) parallel temperature, and (i) ratio of perpendicular temperature to parallel temperature. In the magnetic and electric power spectra (Figures 1b and 1c), enhanced ECH waves are observed within the 1–2 f_{ce} and 2–3 f_{ce} bands during 16:33–16:42 UT, with the fundamental band significantly stronger than the second harmonic. Subsequently, simultaneous enhancements of ECH and chorus waves occur between 16:52 and 17:18 UT. After 17:20 UT, only chorus waves are detected, extending over 0.2–0.7 f_{ce} and exhibiting a distinct power minimum near ~0.5 f_{ce}. During this interval, the spacecraft moves from +1° to −2° in magnetic latitude, likely traversing the equatorial source region and capturing the full temporal evolution of wave activity, from an initial ECH-dominated phase to a period of simultaneous ECH and chorus emissions, followed by a subsequent chorus-dominated phase. This sequence is consistent with the evolution pattern predicted by numerical simulations (Shao et al., 2025). To quantify the overall occurrence characteristics, we performed a statistical survey of all choruses and ECH wave events observed between October 2012 and December 2014. Based on wave amplitude characteristics (Figures 1b and 1e), the events are classified into three categories: ECH-only, chorus-only, and simultaneous chorus and ECH waves. Each 1-min interval is treated as a single event. In total, 8,750 ECH-only events (145.83 hr), 4,215 chorus-only events (70.25 hr), and 12,467 co-occurring events (207.78 hr) were identified during 9,184 hr of total spacecraft observation time.

Figure 2 presents the spatial distributions of wave occurrence rates for the three event categories in both the L–MLT (Figures 2a–2c) and L–MLAT (Figures 2d–2f) planes. Binning was performed with a resolution of 1 hr in MLT by 0.5 in L for the L–MLT projection, and 0.5 in L by 2° in MLAT for the L–MLAT projection. Only bins containing more than 800 1-min samples were retained to ensure statistical reliability. The occurrence rate is defined as the ratio of wave observation time to the total spacecraft dwell time within each bin. When occurring independently (Figures 2a and 2d), chorus waves are mainly observed from midnight through dawn to the noon sector (MLT = 23–13), spanning a wide magnetic latitude range (MLAT = $|2-10|$°) and L-shells between 4 and 6. In contrast, ECH-only events (Figures 2b and 2e) are confined to the midnight sector (MLT = 21–03), concentrated near the magnetic equator (MLAT = ($|0-4|$°)) and at relatively outer L-shells ($5 < L < 6$). Co-occurring events (Figures 2c and 2f) occur most frequently between midnight and dawn (MLT = 21–07), distributed over $-4° <$ MLAT $< 6°$ and $4 < L < 6$. Notably, the occurrence rate of co-occurring events exceeds that of either wave type occurring alone.

Figure 3 maps the mean electric amplitudes of chorus and ECH waves for the three event categories in both the L–MLT and L–MLAT planes. To ensure statistical significance, only bins containing at least 20 wave events were included. For chorus-only events (Figures 3a and 3b), the most intense waves are mainly distributed from midnight to dawn (MLT = 23–10), spanning a broad range of latitudes ($|$MLAT$|$ = 0−12°) and L-shells ($4 < L < 6$). The observed increase in the electric field amplitude at higher latitudes is mainly attributed to oblique propagation effects. As the chorus propagates away from the equatorial generation region, they become increasingly oblique, leading to a relative enhancement of the electric field component (Verkhoglyadova et al., 2010). The corresponding magnetic field amplitude distribution (Figure S1 in Supporting Information S1) shows that intense chorus waves are still observed at higher latitudes, implying that Landau damping decreases with increasing magnetic latitude. This reduced damping allows chorus waves to propagate away from the equatorial source region without severe attenuation, which may help explain the similar occurrence distributions. For ECH-only events (Figures 3e and 3f), strong emissions are confined to the nightside (MLT = 20–07), concentrated near the magnetic equator ($|$MLAT$| < 4°$) and at outer L-shells ($4.5 < L < 6$). Such spatial confinement is consistent with linear theory, which predicts that ECH waves are preferentially generated near the magnetic equator (Ashour-Abdalla & Kennel, 1978). During co-occurring events (Figures 3c, 3d, 3g, and 3h), intense waves are predominantly observed from midnight to dawn (MLT = 21–09) within $4 < L < 6$. In these

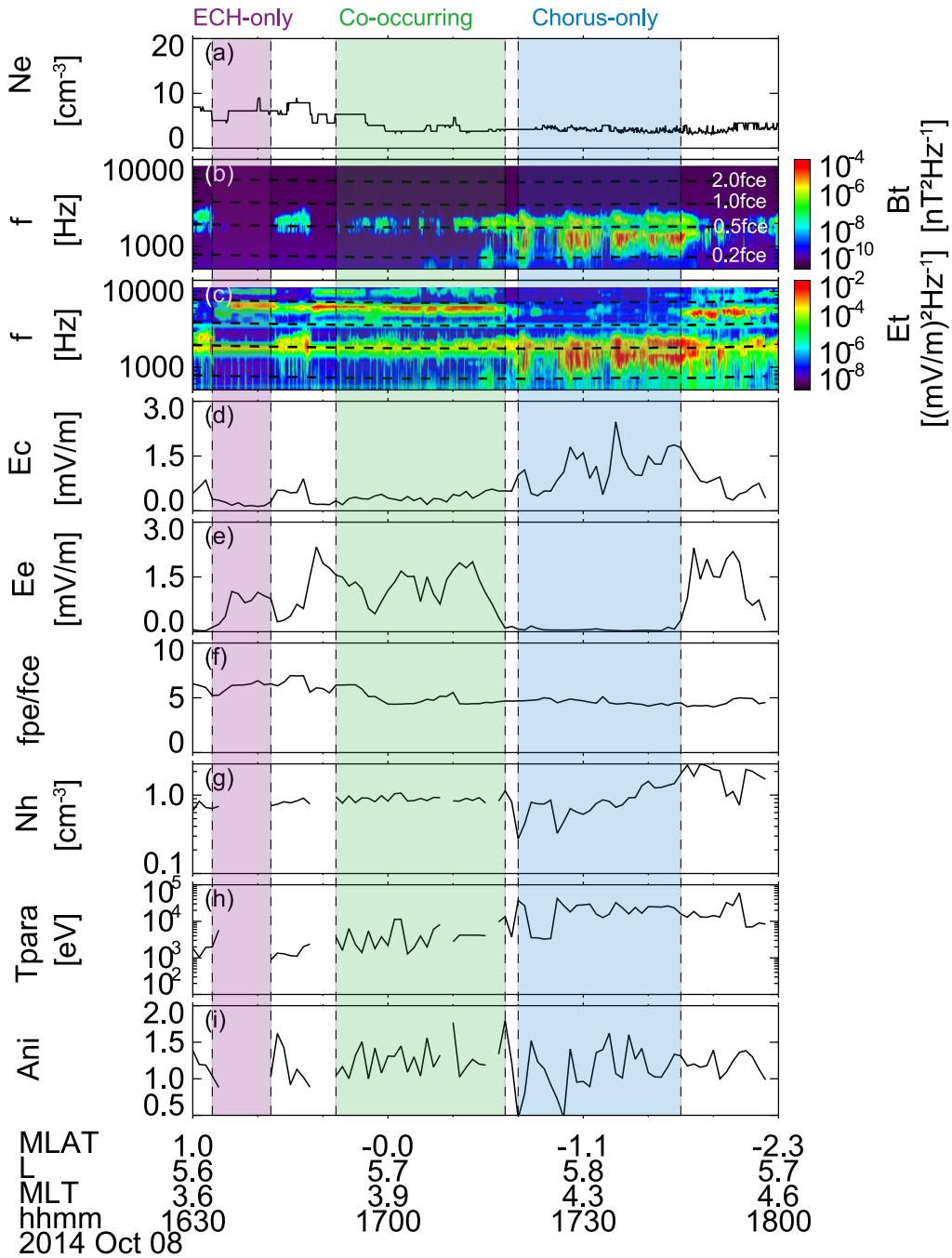

Figure 1. Representative interval of simultaneous chorus and ECH wave observations from Van Allen Probe A on 8 October 2014. From top to bottom: (a) electron density; (b) magnetic field power spectral density; (c) electric field power spectral density; (d) electric amplitude of chorus waves; (e) electric amplitude of ECH waves; (f) ratio of plasma frequency to electron cyclotron frequency; (g) hot electron density; (h) parallel electron temperature; and (i) ratio of perpendicular electron temperature to parallel electron temperature. Three distinct intervals are marked: ECH-only (purple shading), co-occurring waves (green shading), and chorus-only (blue shading). Black dashed lines in panels (b) and (c) denote 0.2 f_{ce}, 0.5 f_{ce}, 1.0 f_{ce} and 2.0 f_{ce}, respectively.

cases, intense chorus waves extend across a wide magnetic latitude range (|MLAT| $= 0-12°$), whereas intense ECH waves remain confined close to the equatorial plane ($-4° <$ MLAT $< 6°$). Overall, co-occurring events exhibit higher wave amplitudes than those where only one wave type is present.

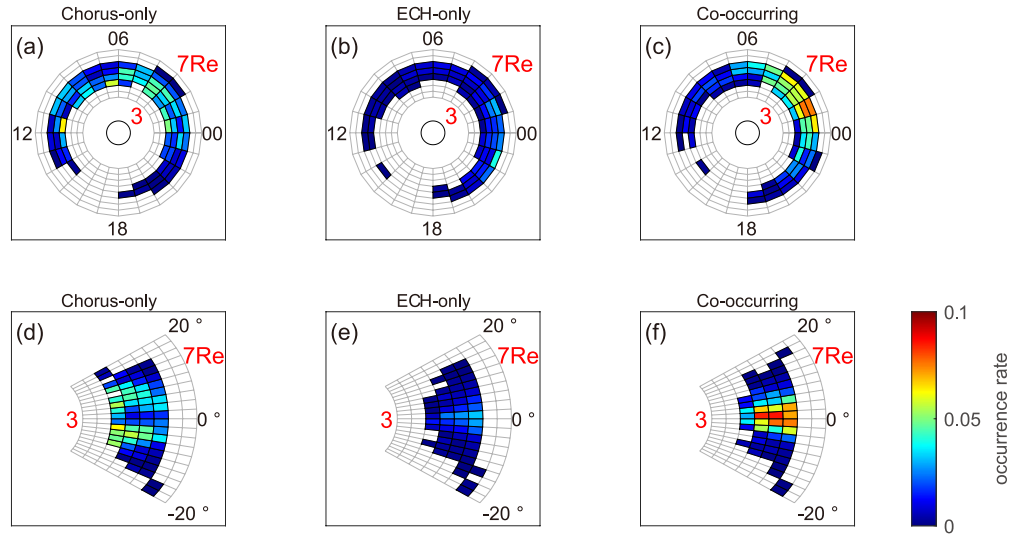

Figure 2. Spatial distribution of occurrence rates for (a, d) chorus-only, (b, e) ECH-only, and (c, f) co-occurring wave events in the (a–c) L–MLT (0.5 L × 1 MLT) and (d–f) L–MLAT (0.5 L × 2 MLAT) planes. Only bins containing more than 800 1-min samples were included to ensure statistical reliability.

To further examine the relationship between chorus and ECH waves during their co-occurrence, Figure 4 compares their electric amplitudes under different magnetic latitude conditions. Figures 4a and 4b show results at higher latitudes ($|\mathrm{MLAT}| > 3°$), while Figures 4c and 4d present those near the magnetic equator ($|\mathrm{MLAT}| \leq 3°$). At higher latitudes, the ECH electric amplitude (E_{ech}) shows no clear trend with the chorus electric amplitude (E_{chorus}; Figure 4a). To minimize potential bias arising from the shared spatial source region, E_{ech} is further examined as a function of the normalized amplitude ratio ($E_{\mathrm{chorus}}/E_{\mathrm{ech}}$, Figure 4b). This analysis reveals a weak anticorrelation between the amplitudes of the two wave types (correlation coefficient $r = -0.26$). Near the magnetic equator, E_{ech} decreases with increasing E_{chorus}, and the normalized amplitude ratio further highlights this anticorrelation ($r = -0.31$, Figures 4c and 4d). It is important to note that this anticorrelation relationship also holds for the magnetic field amplitude of chorus waves. The anticorrelation at higher latitudes likely reflects their spatial separation: chorus waves can propagate away from the equatorial source region without severe attenuation, whereas intense ECH waves remain confined near the equatorial plane. In contrast, the pronounced anticorrelation observed near the magnetic equator suggests an intrinsic interplay between the two wave modes, indicating that local wave–particle interactions govern their relative intensities rather than spatial effects. It is

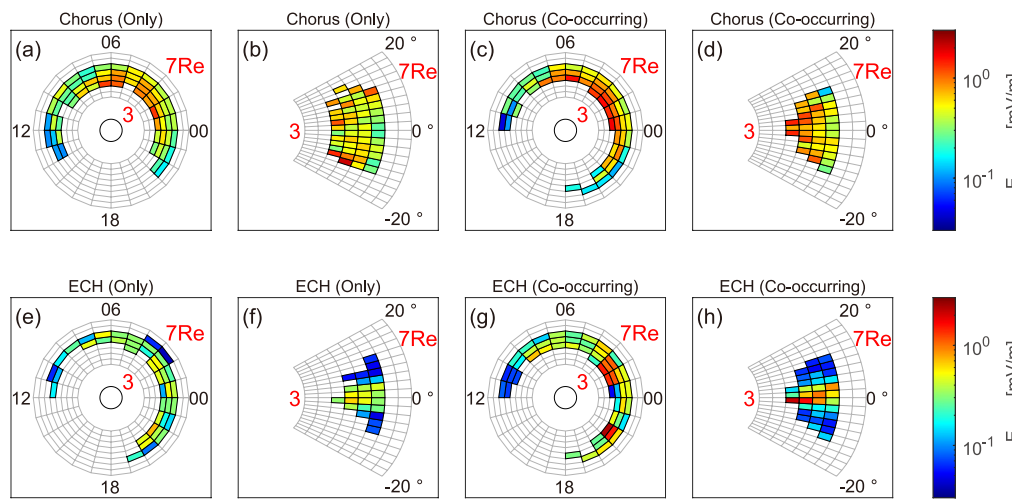

Figure 3. Average electric field amplitudes for (a, b) chorus-only, (c, d, g, h) co-occurring, and (e, f) ECH-only events in the L–MLT and L–MLAT planes. Only bins containing at least 20 wave events were included to ensure statistical significance.

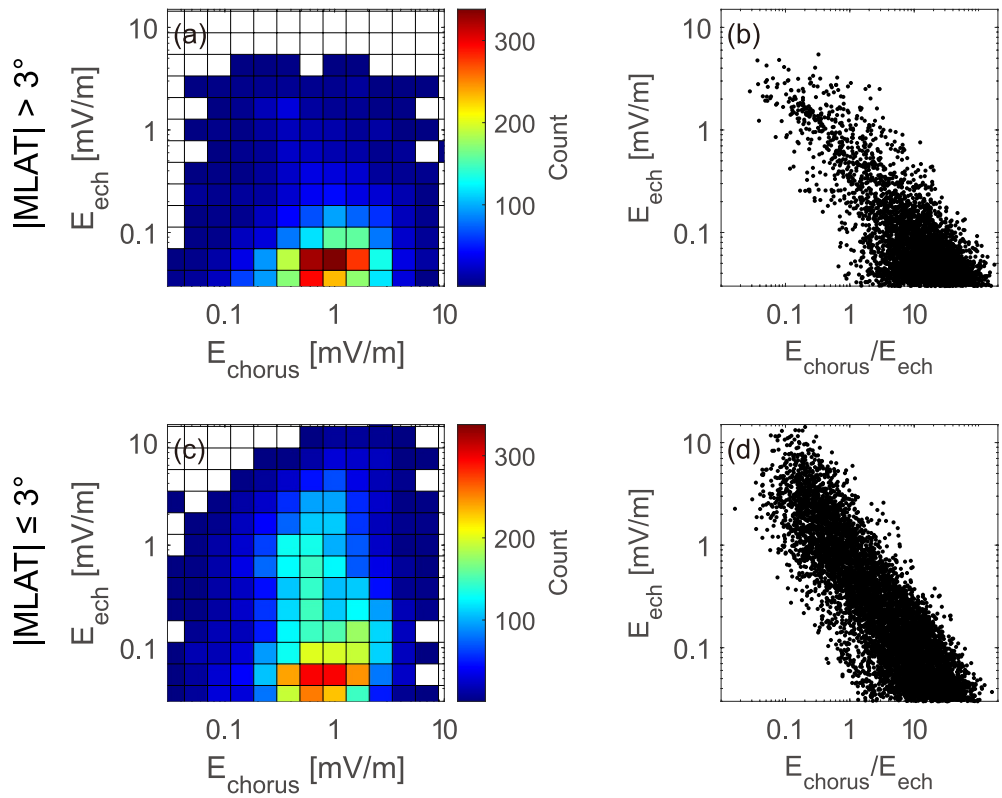

Figure 4. Comparison of chorus (E_{chorus}) and ECH (E_{ech}) wave amplitudes during co-occurring events under different magnetic latitude conditions. Panels (a–b) show results at higher latitudes (|MLAT| > 3°), while panels (c–d) correspond to near-equatorial events (|MLAT| ≤ 3°). Panels (a) and (c) display E_{chorus} as a function of E_{ech}, while Panels (b) and (d) show the relationship between E_{ech} and the normalized amplitude ratio (E_{chorus}/E_{ech}).

worth noting that a direct scatter plot of the absolute amplitudes of chorus and ECH waves does not show significant anticorrelation. This is likely because both wave modes are driven by the same electron injections (Anderson & Maeda, 1977), which tend to enhance both amplitudes simultaneously and mask competitive suppression. Therefore, analyzing the amplitude ratio is essential to reveal the relative dominance of the wave modes.

Figure 5 illustrates the dependence of the wave amplitude ratio (E_{chorus}/E_{ech}) on key plasma parameters near the magnetic equator (|MLAT| ≤ 3°), including f_{pe}/f_{ce}, electron temperature anisotropy, hot electron density, and parallel temperature. As shown in Figure 5a, the amplitude ratio exhibits an inverse correlation with f_{pe}/f_{ce} ($r = -0.194$). A least-squares fit yields the approximate relation: $E_{chorus}/E_{ech} = 10^{6.01} \times \left(f_{pe}/f_{ce}\right)^{-8.06}$. Similarly, Figure 5c shows an inverse correlation between amplitude ratio and hot electron density ($r = -0.136$), described by $E_{chorus}/E_{ech} = 10^{-0.38} \times N_h{}^{-4.47}$. In contrast, the amplitude ratio shows no significant dependence on either the temperature anisotropy ($r = -0.067$) or the parallel temperature ($r = 0.012$). Overall, these results demonstrate that the amplitude ratio decreases with increasing f_{pe}/f_{ce} and hot electron density, while remaining largely insensitive to variations in temperature anisotropy and parallel temperature. These observational trends are consistent with numerical simulations (Shao et al., 2025), further supporting the view that the evolution of the two wave modes is influenced by ambient plasma parameters.

4. Discussion

Chorus and ECH waves are both generated through loss-cone or temperature anisotropy instabilities driven by energetic electrons injected from the plasma sheet (W. Li et al., 2008; Liu et al., 2018). Temperature anisotropy is the dominant source of free energy at large L-shells, while the loss cone instability becomes more significant at small L-shells. As these electrons drift eastward from midnight toward dawn, wave generation occurs

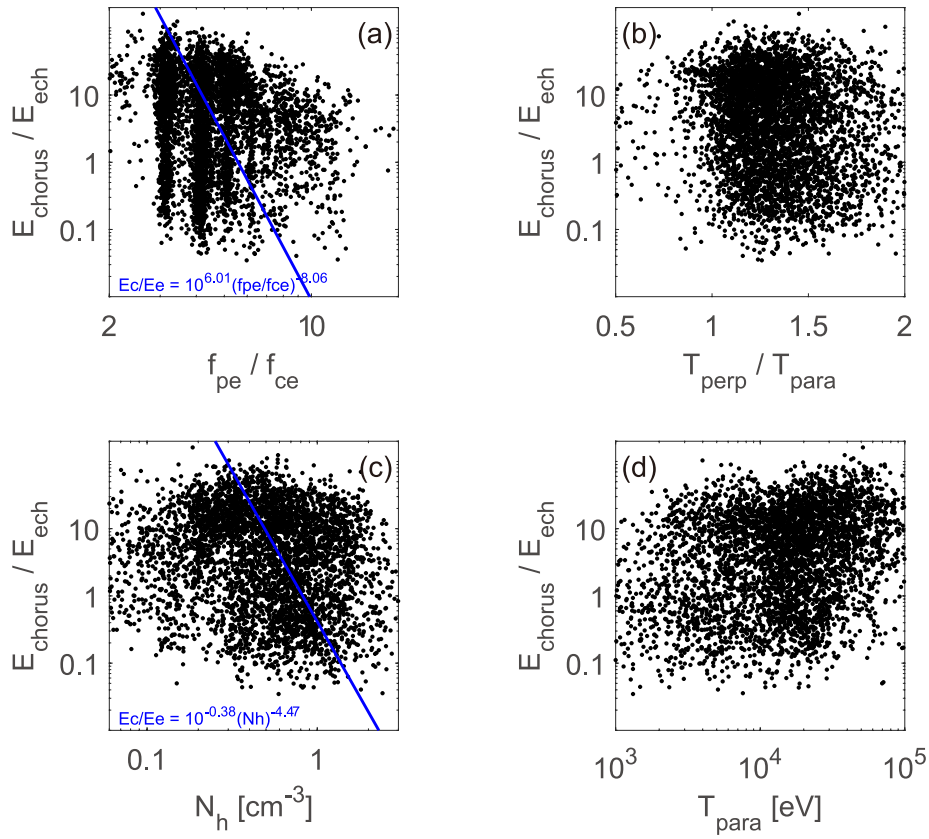

Figure 5. Dependence of the chorus-to-ECH amplitude ratio (E_{chorus}/E_{ech}) on (a) the plasma to cyclotron frequency ratio (f_{pe}/f_{ce}), (b) electron temperature anisotropy, (c) hot electron density, and (d) parallel electron temperature. Solid blue lines in panels (a) and (c) denote the least-squares fits to the data.

correspondingly at these local times (W. Li et al., 2009; Ma et al., 2022; Meredith et al., 2009; Ni et al., 2017). In this study, the spatial distributions of occurrence rates and amplitudes for chorus-only and ECH-only events agree well with previous statistical results (Ma et al., 2022; Meredith et al., 2009; Ni et al., 2017; Tsurutani & Smith, 1977). As shown in Figures 2 and 3, both wave types are predominantly observed in the midnight-to-dawn sector, consistent with the drift paths of injected electrons. Chorus waves, which can propagate along magnetic field lines to higher latitudes, exhibit a broader distribution in MLAT (Lu et al., 2019; Teng et al., 2019), whereas ECH waves, propagating nearly perpendicular to the background magnetic field, remain confined near the magnetic equator (Ashour-Abdalla & Kennel, 1978; Lou et al., 2025; Zhang et al., 2015). Typically, chorus waves exhibit a post-dawn maximum over a broader range of L-shells (Tsurutani & Smith, 1977). However, the electric field amplitude (E_{chorus}) shown in Figure 3 displays a pre-dawn maximum at low L-shells. For chorus-only events, waves in the pre-dawn and low L regions tend to have large wave normal angles (Figure S1 in Supporting Information S1), for which the electric field component is significantly enhanced relative to the magnetic component. In contrast, for co-occurring events, the pre-dawn, low-L wave distribution is likely influenced by magnetic storm dynamics, where strong convection electric fields transport source electrons deep into the magnetosphere. To understand the differences in latitudinal distribution, we examined the local plasma beta conditions. Our statistics show that co-occurring events are associated with much higher plasma beta compared to chorus-only events (Figure S2 in Supporting Information S1). Physically, this suggests that for co-occurring events, the high beta environment leads to stronger Landau damping, confining intense waves near the equatorial source region. Conversely, the lower beta environment of chorus-only event results in weaker damping, allowing waves to propagate to higher latitudes.

The observed anticorrelation between chorus and ECH wave amplitudes reflects distinct physical processes operating at different latitudes. At higher latitudes, the anticorrelation can be attributed to the spatial separation of the two wave populations, as chorus waves are amplified during propagation along magnetic field lines, whereas

ECH waves remain confined near the magnetic equator (Lou et al., 2025; Lu et al., 2019). Near the magnetic equator, where both chorus and ECH waves are locally generated, the pronounced anticorrelation represents an intrinsic interplay between the two wave modes rather than a spatial effect. Consistent with previous studies (Gao et al., 2024), we observed a general inverse correlation between the chorus and ECH wave intensities, suggesting that chorus waves typically suppress ECH waves by consuming the available free energy. However, this suppression mechanism may be regulated by local plasma beta conditions. ECH-only events are favored under lower plasma beta conditions (Figure S2 in Supporting Information S1), where the elevated instability threshold for chorus waves (Gary & Wang, 1996) inhibits their generation, allowing ECH waves to exist without suppression. For chorus-only events, the plasma conditions permit the chorus instability to develop effectively and consume the available free energy, leading to the suppression of ECH waves. Co-occurring events, however, are associated with strong electron injections. In this scenario, the electron free energy is sufficiently high that the chorus instability may saturate, leaving excess free energy to simultaneously drive intense ECH waves. This abundance of free energy also explains why wave amplitudes in co-occurring events are significantly larger than those in single-mode events.

The dependence of the amplitude ratio between chorus and ECH waves (E_{chorus}/E_{ech}) on plasma parameters is broadly consistent with numerical simulations (Shao et al., 2025). Both observations and simulations show that the amplitude ratio decreases with increasing f_{pe}/f_{ce} and hot electron density. This trend likely results from the fact that the minimum resonance energy for both wave modes decreases as f_{pe}/f_{ce} increases, enhancing the linear growth rates of both waves, particularly for ECH waves. Consequently, the amplitude ratio tends to decrease with increasing f_{pe}/f_{ce}. Since f_{pe}/f_{ce} generally increases with L-shell (Angelopoulos et al., 2023), this mechanism also explains why ECH waves are preferentially observed at larger L-shells (Figures 2b and 2e). The vertical clustering of f_{pe}/f_{ce} values in Figure 5a may reflect long-lasting chorus waves that contribute disproportionately to counting at specific f_{pe}/f_{ce} levels. Similarly, as the hot electron density rises, the growth rates of both wave modes are enhanced, but ECH waves experience stronger amplification, leading to a net decrease in E_{chorus}/E_{ech}. It should be noted that the scatter in Figure 5 results in relatively low correlation coefficients. This is expected because the growth rates of chorus and ECH waves are regulated by multiple parameters simultaneously, rather than by the plasma frequency ratio or hot electron density alone. Moreover, satellite observations capture waves after their excitation, which can further increase the variability. Despite these limitations, the statistical trends observed in Figures 5a and 5c remain consistent with theoretical predictions (Shao et al., 2025), supporting the interpretation that plasma frequency ratio and hot electron density are important factors in regulating the amplitude ratio of the two wave modes.

Both observations and simulations indicate that the amplitude ratio depends weakly on the electron parallel temperature (Shao et al., 2025). The growth rates and amplitudes of both wave modes increase with higher parallel temperature, resulting in a nearly constant amplitude ratio. However, our results differ from simulations in that no clear dependence on electron temperature anisotropy is observed. This lack of correlation may result from the rapid relaxation of hot electrons after wave excitation, which can obscure accurate measurements of instantaneous anisotropy. Moreover, although simulations suggest that the amplitude ratio is relatively insensitive to the loss-cone width, this parameter cannot be quantitatively assessed in our study owing to the limited pitch-angle resolution of the available electron velocity distribution data.

5. Summary

This study presents a comprehensive statistical investigation of the relationship between whistler-mode chorus and ECH waves using observations from the Van Allen Probes collected between October 2012 and December 2014. The results show that chorus and ECH waves frequently occur simultaneously near the magnetic equator at $L = 4$–6, predominantly between midnight and dawn (MLT = 21–07). During these co-occurring events, intense chorus waves extend across a broad magnetic latitude range (MLAT = $|0-12|^\circ$), whereas intense ECH waves remain confined near the equatorial region ($-4^\circ < \text{MLAT} < 6^\circ$). Near the magnetic equator, the amplitudes of the two wave modes exhibit a clear inverse correlation, suggesting that they are dynamically coupled rather than independent. Moreover, both the occurrence rate and average amplitude of the co-occurring chorus and ECH waves are higher than those of events where only one wave type is present. Statistical analyses further reveal that the amplitude ratio between chorus and ECH waves decreases with increasing f_{pe}/f_{ce} and hot electron density, while showing little dependence on temperature anisotropy or parallel temperature. These results are broadly in

agreement with numerical simulations, confirming that ambient plasma conditions play a key role in shaping their interaction. These findings provide new statistical evidence for the ubiquity of the chorus–ECH interactions and highlight their importance for electron dynamics in the Earth's magnetosphere.

Conflict of Interest

The authors declare no conflicts of interest relevant to this study.

Data Availability Statement

The Van Allen Probes data used in this study are available at https://spdf.gsfc.nasa.gov/pub/data/rbsp.

Acknowledgments
This research was funded by the NSFC Grants (42322406 and 42230201), the Postdoctoral Fellowship Program of CPSF (GZC20250254), National Key Research and Development Program of China (No. 2022YFA1604600), the "USTC Tang Scholar" program (KY2080000097), the Fundamental Research Funds for the Central Universities (KY2080000063, KY2080000138, and WK2080250227), and National Key R&D Program of China (2025YFF0512500). We also acknowledge the entire Van Allen Probes instrument team.

References

Anderson, R. R., & Maeda, K. (1977). VLF emissions associated with enhanced magnetospheric electrons. *Journal of Geophysical Research*, *82*(1), 135–146. https://doi.org/10.1029/ja082i001p00135

Angelopoulos, V., Zhang, X. J., Artemyev, A. V., Mourenas, D., Tsai, E., Wilkins, C., et al. (2023). Energetic electron precipitation driven by electromagnetic ion cyclotron waves from ELFIN's low altitude perspective. *Space Science Reviews*, *219*(5), 37. https://doi.org/10.1007/s11214-023-00984-w

Ashour-Abdalla, M., & Kennel, C. F. (1978). Nonconvective and convective electron cyclotron harmonic instabilities. *Journal of Geophysical Research*, *83*(A4), 1531–1543. https://doi.org/10.1029/ja083ia04p01531

Blake, J., Carranza, P., Claudepierre, S., Clemmons, J., Crain, W., Jr., Dotan, Y., et al. (2013). The magnetic electron ion spectrometer (MagEIS) instruments aboard the radiation belt storm probes (RBSP) spacecraft. *Space Science Reviews*, *179*(1), 383–421. https://doi.org/10.1007/s11214-013-9991-8

Burtis, W. J., & Helliwell, R. A. (1976). Magnetospheric chorus: Occurrence patterns and normalized frequency. *Planetary and Space Science*, *24*(11), 1007–1024. https://doi.org/10.1016/0032-0633(76)90119-7

Chen, H., Gao, X., Lu, Q., Fan, K., Ke, Y., Wang, X., & Wang, S. (2022). Gap formation around $0.5\Omega_e$ in the whistler-mode waves due to the plateau-like shape in the parallel electron distribution: 2D PIC simulations. *Journal of Geophysical Research: Space Physics*, *127*(5), e2021JA030119. https://doi.org/10.1029/2021ja030119

Chen, H., Gao, X., Lu, Q., Sauer, K., Chen, R., Yao, J., & Wang, S. (2021). Gap formation around $0.5\Omega_e$ of whistler-mode waves excited by electron temperature anisotropy. *Journal of Geophysical Research: Space Physics*, *126*(2), e2020JA028631. https://doi.org/10.1029/2020ja028631

Chen, R., Miyoshi, Y., Gao, X., Lu, Q., Tsurutani, B. T., Hosokawa, K., et al. (2024). Observational evidence for three time-scale modulations in the pulsating aurora. *Geophysical Research Letters*, *51*(16), e2024GL108253. https://doi.org/10.1029/2024gl108253

DeForest, S. E., & McIlwain, C. E. (1971). Plasma clouds in the magnetosphere. *Journal of Geophysical Research*, *76*(16), 3587–3611. https://doi.org/10.1029/ja076i016p03587

Feng, H., Wang, D., Guo, D., Shprits, Y. Y., Han, D., Teng, S., et al. (2024). Lower band chorus wave scattering causing the extensive morningside diffuse auroral precipitation during active geomagnetic conditions: A detailed case study. *Journal of Geophysical Research: Space Physics*, *129*(5), e2023JA032240. https://doi.org/10.1029/2023ja032240

Fredricks, R. W., & Scarf, F. L. (1973). Recent studies of magnetospheric electric field emissions above the electron gyrofrequency. *Journal of Geophysical Research*, *78*(1), 310–314. https://doi.org/10.1029/ja078i001p00310

Fukizawa, M., Sakanoi, T., Miyoshi, Y., Kazama, Y., Katoh, Y., Kasahara, Y., et al. (2020). Pitch-angle scattering of inner magnetospheric electrons caused by ECH waves obtained with the Arase satellite. *Geophysical Research Letters*, *47*(23), e2020GL089926. https://doi.org/10.1029/2020gl089926

Funsten, H. O., Skoug, R. M., Guthrie, A. A., MacDonald, E. A., Baldonado, J. R., Harper, R. W., et al. (2013). Helium, oxygen, proton, and electron (HOPE) mass spectrometer for the Radiation Belt Storm Probes Mission. *Space Science Reviews*, *179*(1–4), 423–484. https://doi.org/10.1007/s11214-013-9968-7

Gao, X., Chen, R., Lu, Q., Chen, L., Chen, H., & Wang, X. (2022). Observational evidence for the origin of repetitive chorus emissions. *Geophysical Research Letters*, *49*(12), e2022GL099000. https://doi.org/10.1029/2022gl099000

Gao, X., Li, W., Thorne, R. M., Bortnik, J., Angelopoulos, V., Lu, Q., et al. (2014). New evidence for generation mechanisms of discrete and hiss-like whistler mode waves. *Geophysical Research Letters*, *41*(14), 4805–4811. https://doi.org/10.1002/2014gl060707

Gao, X., Ma, J., Shao, T., Chen, R., Ke, Y., & Lu, Q. (2024). Why chorus waves are the dominant driver for diffuse auroral precipitation. *Science Bulletin*, *69*(5), 597–600. https://doi.org/10.1016/j.scib.2023.12.009

Gary, S. P., & Wang, J. (1996). Whistler instability: Electron anisotropy upper bound. *Journal of Geophysical Research*, *101*(A5), 10749–10754. https://doi.org/10.1029/96ja00323

Helliwell, R. A. (1967). A theory of discrete VLF emissions from the magnetosphere. *Journal of Geophysical Research*, *72*(19), 4773–4790. https://doi.org/10.1029/jz072i019p04773

Horne, R. B., Christiansen, P. J., Gough, M. P., Rönnmark, K. G., Johnson, J. F. E., Sojka, J., & Wrenn, G. L. (1981). Amplitude variations of electron cyclotron harmonic waves. *Nature*, *294*(5839), 338–340. https://doi.org/10.1038/294338a0

Horne, R. B., Thorne, R. M., Meredith, N. P., & Anderson, R. R. (2003). Diffuse auroral electron scattering by electron cyclotron harmonic and whistler mode waves during an isolated substorm. *Journal of Geophysical Research*, *108*(A7). https://doi.org/10.1029/2002ja009736

Horne, R. B., Thorne, R. M., Shprits, Y. Y., Meredith, N. P., Glauert, S. A., Smith, A. J., et al. (2005). Wave acceleration of electrons in the Van Allen radiation belts. *Nature*, *437*(7056), 227–230. https://doi.org/10.1038/nature03939

Ke, Y., Lu, Q., Gao, X., Wang, X., Chen, L., Wang, S., & Wang, S. (2020). Particle-in-cell simulations of characteristics of rising-tone chorus waves in the inner magnetosphere. *Journal of Geophysical Research: Space Physics*, *125*(7), e2020JA027961. https://doi.org/10.1029/2020ja027961

Kennel, C. F., Scarf, F. L., Fredricks, R. W., McGehee, J. H., & Coroniti, F. V. (1970). VLF electric field observations in the magnetosphere. *Journal of Geophysical Research*, *75*(31), 6136–6152. https://doi.org/10.1029/ja075i031p06136

Kessel, R., Fox, N., & Weiss, M. (2013). The radiation belt storm probes (RBSP) and space weather. *Space Science Reviews*, *179*(1), 531–543. https://doi.org/10.1007/s11214-012-9953-6

Kletzing, C. A., Kurth, W., Acuna, M., MacDowall, R., Torbert, R., Averkamp, T., et al. (2013). The electric and magnetic field instrument suite and integrated science (EMFISIS) on RBSP. *Space Science Reviews*, *179*(1), 127–181. https://doi.org/10.1007/s11214-013-9993-6

Kubota, Y., Omura, Y., Kletzing, C., & Reeves, G. (2018). Generation process of large-amplitude upper-band chorus emissions observed by Van Allen Probes. *Journal of Geophysical Research: Space Physics*, *123*(5), 3704–3713. https://doi.org/10.1029/2017ja024782

Kurth, W. S., De Pascuale, S., Faden, J. B., Kletzing, C. A., Hospodarsky, G. B., Thaller, S., & Wygant, J. R. (2015). Electron densities inferred from plasma wave spectra obtained by the Waves instrument on Van Allen Probes. *Journal of Geophysical Research: Space Physics*, *120*(2), 904–914. https://doi.org/10.1002/2014ja020857

LeDocq, M. J., Gurnett, D. A., & Hospodarsky, G. B. (1998). Chorus source locations from VLF Poynting flux measurements with the Polar spacecraft. *Geophysical Research Letters*, *25*(21), 4063–4066. https://doi.org/10.1029/1998gl900071

Li, J., Bortnik, J., Li, W., An, X., Lyons, L. R., Kurth, W. S., et al. (2022). Unraveling the formation region and frequency of chorus spectral gaps. *Geophysical Research Letters*, *49*(19), e2022GL100385. https://doi.org/10.1029/2022gl100385

Li, W., Thorne, R. M., Angelopoulos, V., Bortnik, J., Cully, C. M., Ni, B., et al. (2009). Global distribution of whistler-mode chorus waves observed on the THEMIS spacecraft. *Geophysical Research Letters*, *36*(9). https://doi.org/10.1029/2009gl037595

Li, W., Thorne, R. M., Bortnik, J., Tao, X., & Angelopoulos, V. (2012). Characteristics of hiss-like and discrete whistler-mode emissions. *Geophysical Research Letters*, *39*(18). https://doi.org/10.1029/2012gl053206

Li, W., Thorne, R. M., Meredith, N. P., Horne, R. B., Bortnik, J., Shprits, Y. Y., & Ni, B. (2008). Evaluation of whistler mode chorus amplification during an injection event observed on CRRES. *Journal of Geophysical Research*, *113*(A9). https://doi.org/10.1029/2008ja013129

Liu, X., Chen, L., Gu, W., & Zhang, X. J. (2018). Electron cyclotron harmonic wave instability by loss cone distribution. *Journal of Geophysical Research: Space Physics*, *123*(11), 9035–9044. https://doi.org/10.1029/2018ja025925

Lou, Y., Cao, X., Ni, B., Tu, W., Gu, X., Fu, S., et al. (2021). Diffuse auroral electron scattering by electrostatic electron cyclotron harmonic waves in the dayside magnetosphere. *Geophysical Research Letters*, *48*(5), e2020GL092208. https://doi.org/10.1029/2020gl092208

Lou, Y., Ni, B., Cao, X., Ma, Q., Miyoshi, Y., Wang, D., et al. (2025). Distinct global distribution of electrostatic electron cyclotron harmonic waves in Earth's magnetosphere revealed by multi-satellite observations. *Geophysical Research Letters*, *52*(17), e2025GL117276. https://doi.org/10.1029/2025GL117276

Lu, Q., Chen, L., Wang, X., Gao, X., Lin, Y., & Wang, S. (2021). Repetitive emissions of rising-tone chorus waves in the inner magnetosphere. *Geophysical Research Letters*, *48*(15), e2021GL094979. https://doi.org/10.1029/2021GL094979

Lu, Q., Ke, Y., Wang, X., Liu, K., Gao, X., Chen, L., & Wang, S. (2019). Two-dimensional gcPIC simulation of rising-tone chorus waves in a dipole magnetic field. *Journal of Geophysical Research: Space Physics*, *124*(6), 4157–4167. https://doi.org/10.1029/2019ja026586

Ma, J., Gao, X., Chen, H., Tsurutani, B. T., Ke, Y., Chen, R., & Lu, Q. (2022). The effects of substorm injection of energetic electrons and enhanced solar wind ram pressure on whistler-mode chorus waves: A statistical study. *Journal of Geophysical Research: Space Physics*, *127*(11), e2022JA030502. https://doi.org/10.1029/2022ja030502

Mauk, B. H., Fox, N. J., Kanekal, S. G., Kessel, R. L., Sibeck, D. G., & Ukhorskiy, A. (2012). Science objectives and rationale for the Radiation Belt Storm Probes Mission. *Space Science Reviews*, *179*(1–4), 3–27. https://doi.org/10.1007/s11214-012-9908-y

Meredith, N. P., Horne, R. B., Thorne, R. M., & Anderson, R. R. (2003). Favored regions for chorus-driven electron acceleration to relativistic energies in the Earth's outer radiation belt. *Geophysical Research Letters*, *30*(16). https://doi.org/10.1029/2003gl017698

Meredith, N. P., Horne, R. B., Thorne, R. M., & Anderson, R. R. (2009). Survey of upper band chorus and ECH waves: Implications for the diffuse aurora. *Journal of Geophysical Research*, *114*(A7). https://doi.org/10.1029/2009ja014230

Ni, B., Gu, X., Fu, S., Xiang, Z., & Lou, Y. (2017). A statistical survey of electrostatic electron cyclotron harmonic waves based on THEMIS FFF wave data. *Journal of Geophysical Research: Space Physics*, *122*(3), 3342–3353. https://doi.org/10.1002/2016ja023433

Ni, B., Liang, J., Thorne, R. M., Angelopoulos, V., Horne, R. B., Kubyshkina, M., et al. (2012). Efficient diffuse auroral electron scattering by electrostatic electron cyclotron harmonic waves in the outer magnetosphere: A detailed case study. *Journal of Geophysical Research*, *117*(A1). https://doi.org/10.1029/2011ja017095

Ni, B., Thorne, R. M., Zhang, X., Bortnik, J., Pu, Z., Xie, L., et al. (2016). Origins of the Earth's diffuse auroral precipitation. *Space Science Reviews*, *200*(1–4), 205–259. https://doi.org/10.1007/s11214-016-0234-7

Nishimura, Y., Bortnik, J., Li, W., Thorne, R. M., Lyons, L. R., Angelopoulos, V., et al. (2010). Identifying the driver of pulsating aurora. *Science*, *330*(6000), 81–84. https://doi.org/10.1126/science.1193186

Omura, Y. (2021). Nonlinear wave growth theory of whistler-mode chorus and hiss emissions in the magnetosphere. *Earth Planets and Space*, *73*(1), 95. https://doi.org/10.1186/s40623-021-01380-w

Omura, Y., Katoh, Y., & Summers, D. (2008). Theory and simulation of the generation of whistler-mode chorus. *Journal of Geophysical Research*, *113*(A4). https://doi.org/10.1029/2007ja012622

Shao, T., Gao, X., Ke, Y., Ma, J., Lei, W., & Lu, Q. (2025). Parametric study on the interplay between ECH and whistler waves: Particle-in-cell simulations. *Journal of Geophysical Research: Space Physics*, *130*(7), e2025JA033980. https://doi.org/10.1029/2025ja033980

Sheeley, B. W., Moldwin, M. B., Rassoul, H. K., & Anderson, R. R. (2001). An empirical plasmasphere and trough density model: CRRES observations. *Journal of Geophysical Research*, *106*(A11), 25631–25641. https://doi.org/10.1029/2000ja000286

Spence, H. E., Reeves, G. D., Baker, D., Blake, J., Bolton, M., Bourdarie, S., et al. (2013). Science goals and overview of the radiation belt storm probes (RBSP) energetic particle, composition, and thermal plasma (ECT) suite on NASA's Van Allen probes mission. *Space Science Reviews*, *179*(1), 311–336. https://doi.org/10.1007/s11214-013-0007-5

Stix, T. H., & Scott, F. R. (1963). The theory of plasma waves. *American Journal of Physics*, *31*(10), 816. https://doi.org/10.1119/1.1969127

Tao, X., Zonca, F., Chen, L., & Wu, Y. (2019). Theoretical and numerical studies of chorus waves: A review. *Science China Earth Sciences*, *63*(1), 78–92. https://doi.org/10.1007/s11430-019-9384-6

Teng, S., Tao, X., & Li, W. (2019). Typical characteristics of whistler mode waves categorized by their spectral properties using Van Allen Probes Observations. *Geophysical Research Letters*, *46*(7), 3607–3614. https://doi.org/10.1029/2019gl082161

Thorne, R. M., Li, W., Ni, B., Ma, Q., Bortnik, J., Chen, L., et al. (2013). Rapid local acceleration of relativistic radiation-belt electrons by magnetospheric chorus. *Nature*, *504*(7480), 411–414. https://doi.org/10.1038/nature12889

Thorne, R. M., Ni, B., Tao, X., Horne, R. B., & Meredith, N. P. (2010). Scattering by chorus waves as the dominant cause of diffuse auroral precipitation. *Nature*, *467*(7318), 943–946. https://doi.org/10.1038/nature09467

Tsurutani, B. T., Lakhina, G. S., & Verkhoglyadova, O. P. (2013). Energetic electron (>10 keV) microburst precipitation, ~5–15 s X-ray pulsations, chorus, and wave-particle interactions: A review. *Journal of Geophysical Research: Space Physics*, *118*(5), 2296–2312. https://doi.org/10.1002/jgra.50264

Tsurutani, B. T., Chen, R., Gao, X., Lu, Q., Pickett, J. S., Lakhina, G. S., et al. (2020). Lower-band "Monochromatic" chorus riser subelement/wave packet observations. *Journal of Geophysical Research: Space Physics*, *125*(10), e2020JA028090. https://doi.org/10.1029/2020ja028090

Tsurutani, B. T., & Smith, E. J. (1974). Postmidnight chorus: A substorm phenomenon. *Journal of Geophysical Research*, *79*(1), 118–127. https://doi.org/10.1029/ja079i001p00118

Tsurutani, B. T., & Smith, E. J. (1977). Two types of magnetospheric ELF chorus and their substorm dependences. *Journal of Geophysical Research*, *82*(32), 5112–5128. https://doi.org/10.1029/ja082i032p05112

Tsurutani, B. T., Smith, E. J., West, H. I., & Buck, R. M. (1979). Chorus, energetic electrons and magnetospheric substorms. In *Paper presented at wave instabilities in space plasmas*. Springer Netherlands.

Tsyganenko, N. A., & Sitnov, M. I. (2005). Modeling the dynamics of the inner magnetosphere during strong geomagnetic storms. *Journal of Geophysical Research*, *110*(A3). https://doi.org/10.1029/2004ja010798

Tu, W., Cunningham, G. S., Chen, Y., Morley, S. K., Reeves, G. D., Blake, J. B., et al. (2014). Event-specific chorus wave and electron seed population models in DREAM3D using the Van Allen Probes. *Geophysical Research Letters*, *41*(5), 1359–1366. https://doi.org/10.1002/2013gl058819

Verkhoglyadova, O. P., Tsurutani, B. T., & Lakhina, G. S. (2010). Properties of obliquely propagating chorus. *Journal of Geophysical Research*, *115*(A9). https://doi.org/10.1029/2009ja014809

Wang, D., & Shprits, Y. Y. (2019). On how high-latitude chorus waves tip the balance between acceleration and loss of relativistic electrons. *Geophysical Research Letters*, *46*(14), 7945–7954. https://doi.org/10.1029/2019gl082681

Wang, D., Shprits, Y. Y., Zhelavskaya, I. S., Agapitov, O. V., Drozdov, A. Y., & Aseev, N. A. (2019). Analytical chorus wave model derived from Van Allen Probe Observations. *Journal of Geophysical Research: Space Physics*, *124*(2), 1063–1084. https://doi.org/10.1029/2018ja026183

Wu, Y., Tao, X., Liu, X., Chen, L., Xie, H., Liu, K., & Horne, R. B. (2020). Particle-in-cell simulation of electron cyclotron harmonic waves driven by a loss cone distribution. *Geophysical Research Letters*, *47*(9), e2020GL087649. https://doi.org/10.1029/2020gl087649

Xiao, F., Yang, C., He, Z., Su, Z., Zhou, Q., He, Y., et al. (2014). Chorus acceleration of radiation belt relativistic electrons during March 2013 geomagnetic storm. *Journal of Geophysical Research: Space Physics*, *119*(5), 3325–3332. https://doi.org/10.1002/2014ja019822

Zhang, X. J., Angelopoulos, V., Ni, B., & Thorne, R. M. (2015). Predominance of ECH wave contribution to diffuse aurora in Earth's outer magnetosphere. *Journal of Geophysical Research: Space Physics*, *120*(1), 295–309. https://doi.org/10.1002/2014ja020455